

Crystal structure of the ATP-gated P2X4 ion channel in the closed state

Toshimitsu Kawate¹, Jennifer Carlisle Michel¹, William T. Birdsong¹ & Eric Gouaux^{1,2}

¹Vollum Institute and ²Howard Hughes Medical Institute, Oregon Health and Science University, 3181 SW Sam Jackson Park Road, OR 97239, USA

Table of Contents

	Page
Supplementary Table 1. Data collection statistics	2
Supplementary Table 2. Crystallographic refinement statistics	3
Supplementary Fig. 1. P2X receptors are glycosylated and tend to aggregate	4
Supplementary Fig. 2. ATP dose-dependent activation and expression levels of zfp2X constructs	5
Supplementary Fig. 3. Sequence alignment	6-9
Supplementary Fig. 4. Crystal packing of Δ zfp2X4	10
Supplementary Fig. 5. Anomalous difference Fourier maps from selenomethionine derivatives of Δ zfp2X4-A	11
Supplementary Fig. 6. Electron densities in the transmembrane region	12
Supplementary Fig. 7. Stereoview of the three subunit superposition	13
Supplementary Fig. 8. Stereoview of the subunit superposition between Δ zfp2X4-A and Δ zfp2X4-B	14
Supplementary Fig. 9. Sequence and features of the two deletion constructs used in the current structural study	15
Supplementary Fig. 10. Locations of variable residues	16
Supplementary Fig. 11. Extracellular vestibules and the ion channel domain	17
Supplementary Fig. 12. Gadolinium inhibition depends on ATP concentration	18
Supplementary Fig. 13. Side chain density in the ATP-binding pocket viewed $\sim 90^\circ$ from Figure 6b	19

Supplementary Table 1. Data collection statistics

Dataset	Native (A ^a)	Native (B ^b)	Native (A -low energy-)	Gd ^c (A)
Space group	R3	R32	R3	R3
Wavelength (Å)	1.0000	1.0000	1.6000	1.5629
Cell (a x c) (Å) ^d	234.9 x 138.4	100.8 x 431.3	235.0 x 138.9	236.3 x 138.7
Resolution (Å)	50-3.46 (3.52-3.46)	50-3.09 (3.20-3.09) ^e	50-5.0 (5.09-5.00)	50-4.2 (4.27-4.20)
Completeness (%)	99.9 (99.8)	90.1 (69.9)	98.8 (88.0)	99.6 (98.3)
Redundancy	5.0 (5.0)	3.3 (2.8)	3.7 (2.9)	3.6 (3.0)
Rmerge (%)	5.3 (79.1)	8.0 (48.4)	2.9 (31.2)	4.0 (39.8)
I/σI	18.1 (1.4)	18.2 (1.8)	20.1 (2.1)	17.0 (1.8)

Dataset	Se ^f (A)	Se-C51M ^g (A)	Se-L349M ^h (A)
Space group	R3	R3	R3
Wavelength (Å)	0.9787	0.9787	0.9786
Cell (a x c) (Å)	234.6 x 138.4	235.4 x 138.7	236.6 x 139.6
Resolution (Å)	50-4.6 (4.68-4.60)	50-3.36 (3.42-3.36)	50-4.2 (4.27-4.20)
Completeness (%)	99.6 (95.3)	97.1 (83.1)	99.8 (99.7)
Redundancy	6.8 (5.1)	7.1 (4.9)	6.3 (5.6)
Rmerge (%)	2.5 (44.0)	6.0 (57.7)	4.9 (53.7)
I/σI	19.3 (1.8)	19.5 (1.4)	19.9 (1.9)

^aΔzfP2X4-A (ΔN27/ΔC8).

^bΔzfP2X4-B (ΔN27/ΔC8/C51F/N78K/N187R).

^cDerivative data set from a crystal grown in the presence of GdCl₃.

^dHexagonal setting.

^eValues for the highest resolution shell are shown in parentheses.

^fData set from a SeMet derivative crystal of the parent ΔzfP2X4-A construct.

^gData set from a SeMet derivative crystal of the ΔzfP2X4-A (C51M) mutant.

^hData set from a SeMet derivative crystal of the ΔzfP2X4-A (L349M) mutant.

Supplementary Table 2. Crystallographic refinement statistics

Phasing

Figure of merit	0.34
NCS correlation (%) ^a	78.4

Refinement

Data	Native (A ^b)	Native (B ^c)
Resolution range (Å)	47.74-3.46	29.11-3.10
R _{work} /R _{free}	0.277/ 0.289	0.248/ 0.278
Number of reflections	32647	14372
Completeness (%)	87.8 ^d	90.7 ^e
Number of atoms	7294	2500
RMSD bond (Å)	0.007	0.008
RMSD angle (°)	1.272	1.483
Average B-factor (Å ²)	126.1	105.4
Ramachandran plot		
Favoured (%)	85.4	86.3
Allowed (%)	14.6	13.7
Generously allowed (%)	0	0
Disallowed (%)	0	0

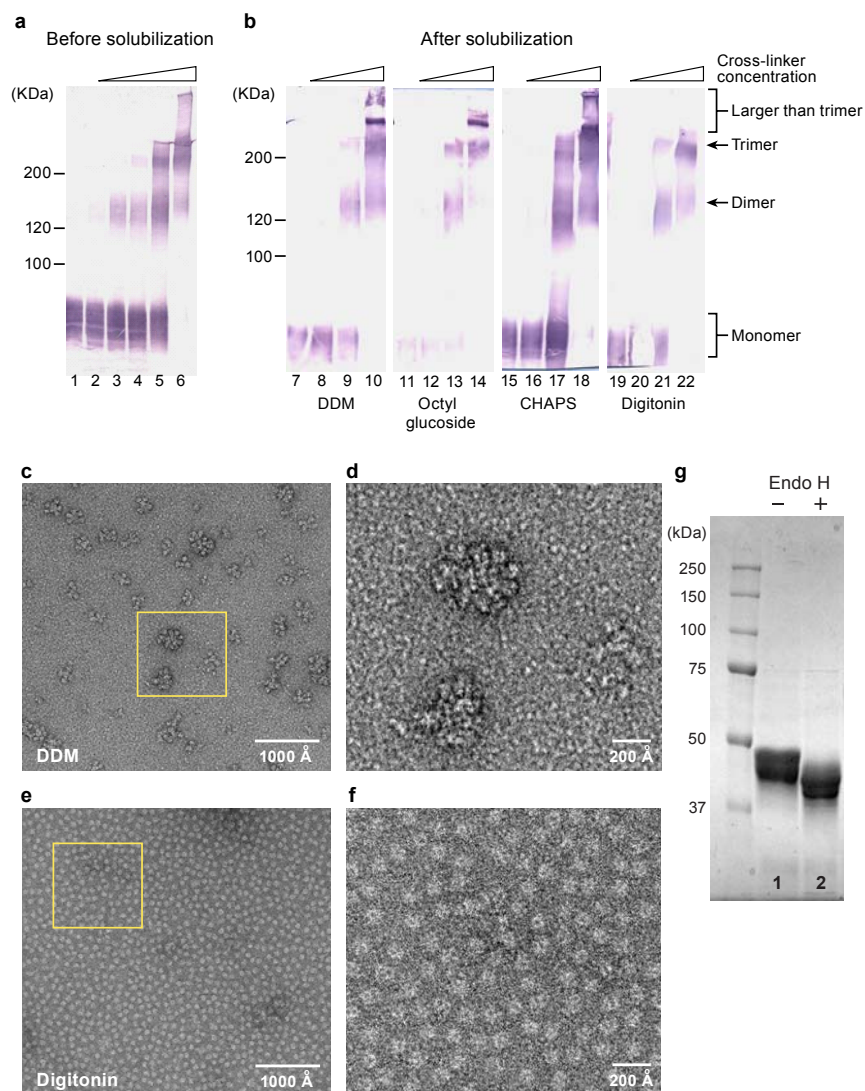
^aCorrelation between the electron density areas related by non-crystallographic symmetry.

^b $\Delta_{zf}P2X4-A$ ($\Delta N27/\Delta C8$).

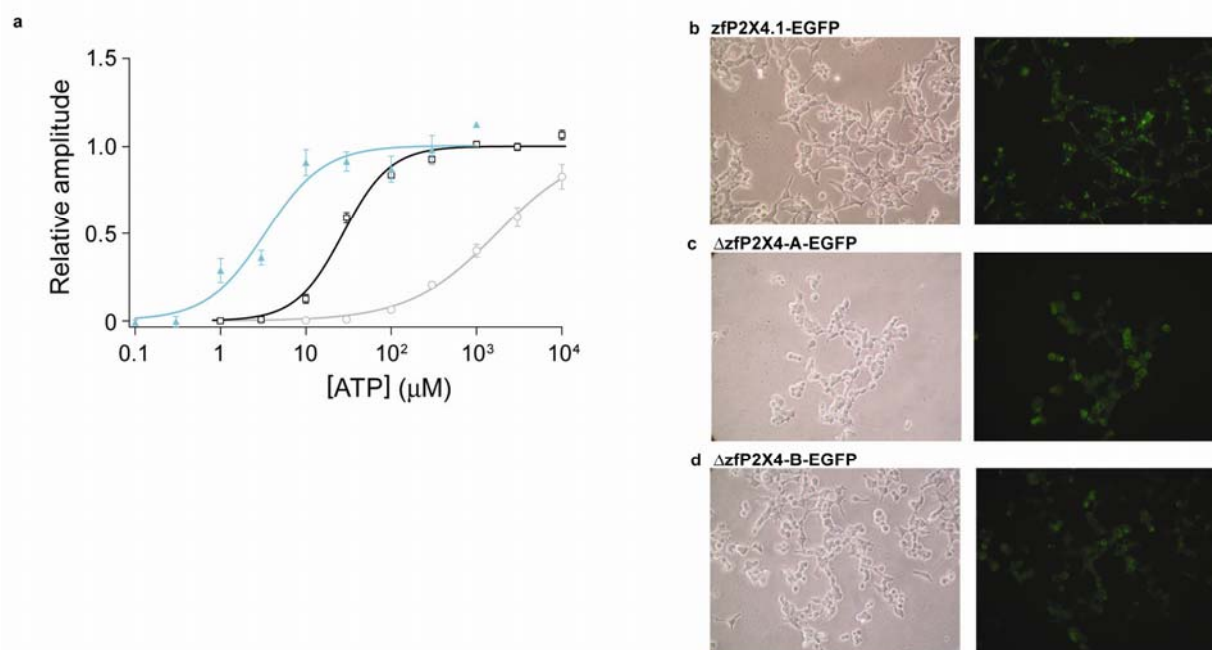
^c $\Delta_{zf}P2X4-B$ ($\Delta N27/\Delta C8/C51F/N78K/N187R$).

^dF_{obs} ≤ 0 were excluded from the refinement (6073 out of 37125 reflections in 47.73-3.30 Å). 4.8% of the reflections were excluded from the refinement for R_{free} calculation.

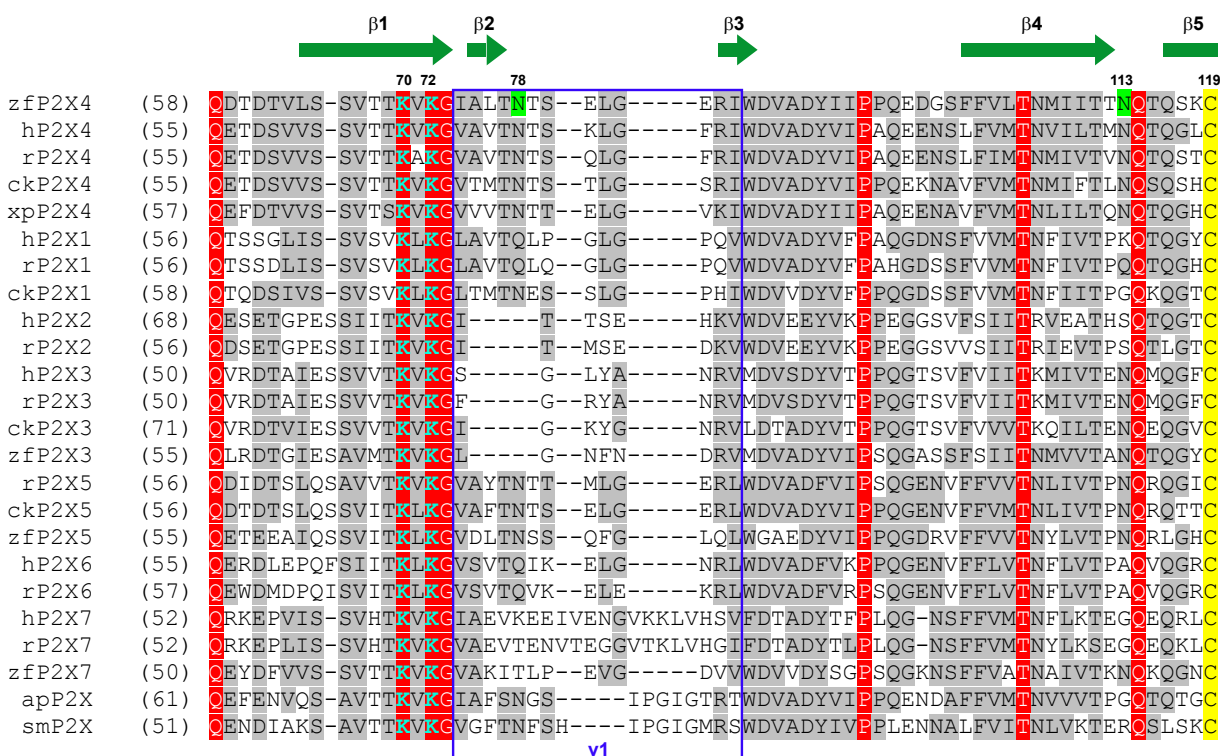
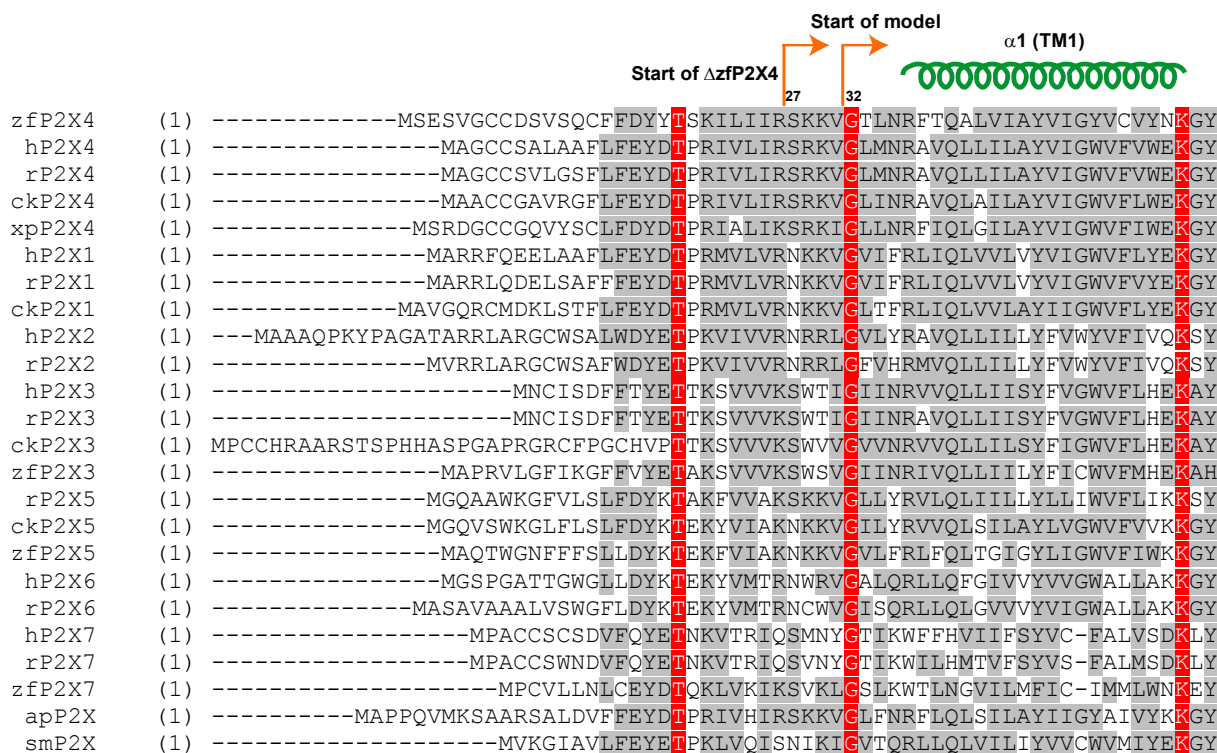
^e5.1% of the reflections were excluded from the refinement for R_{free} calculation.

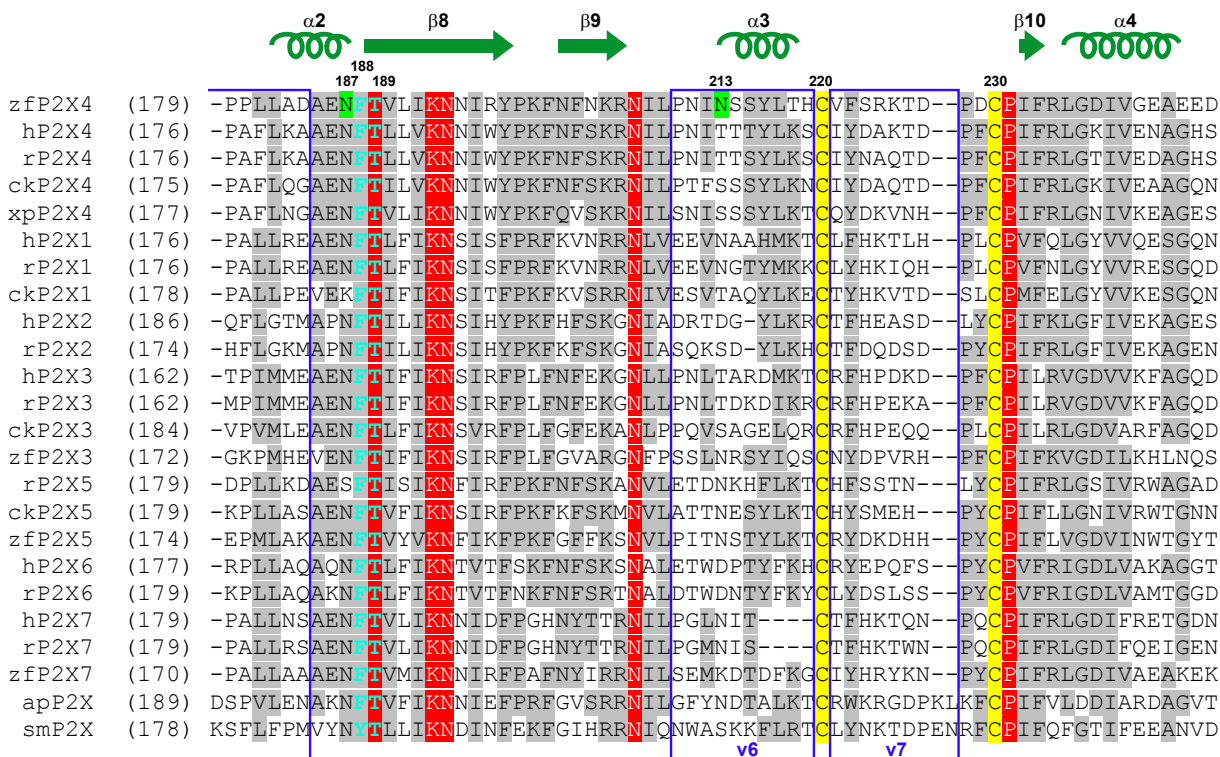
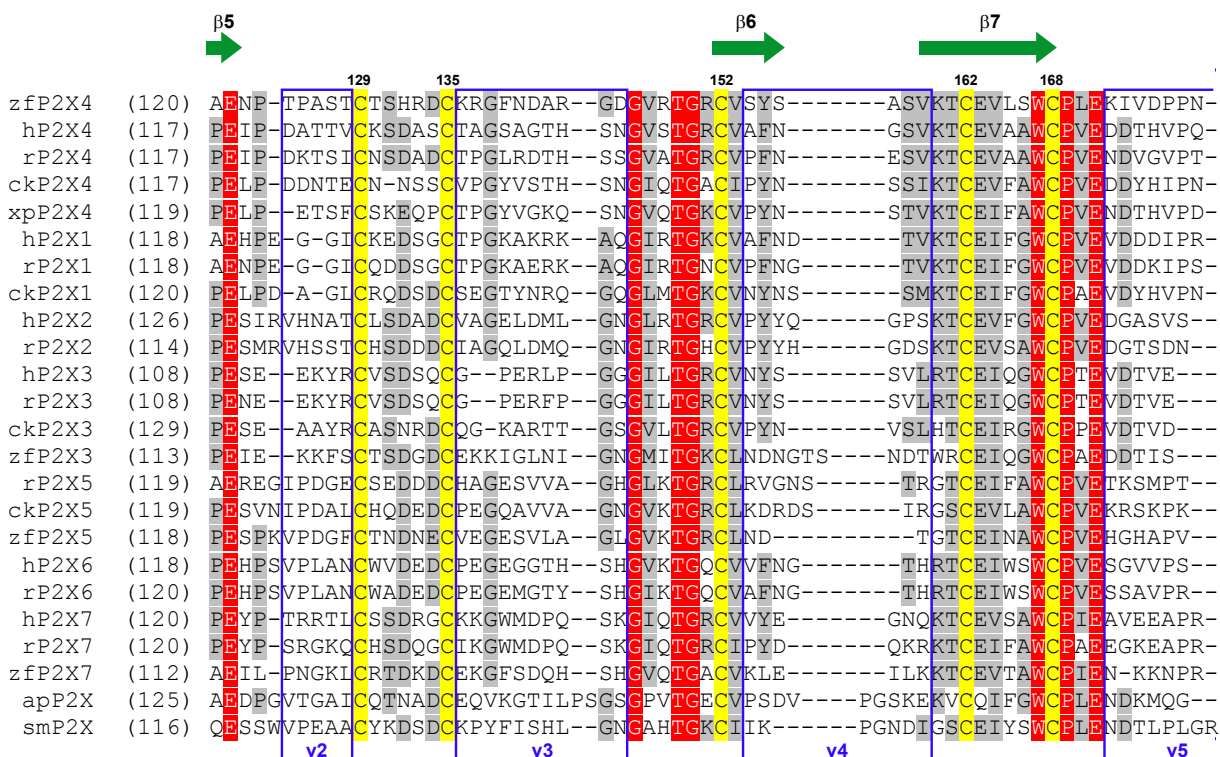


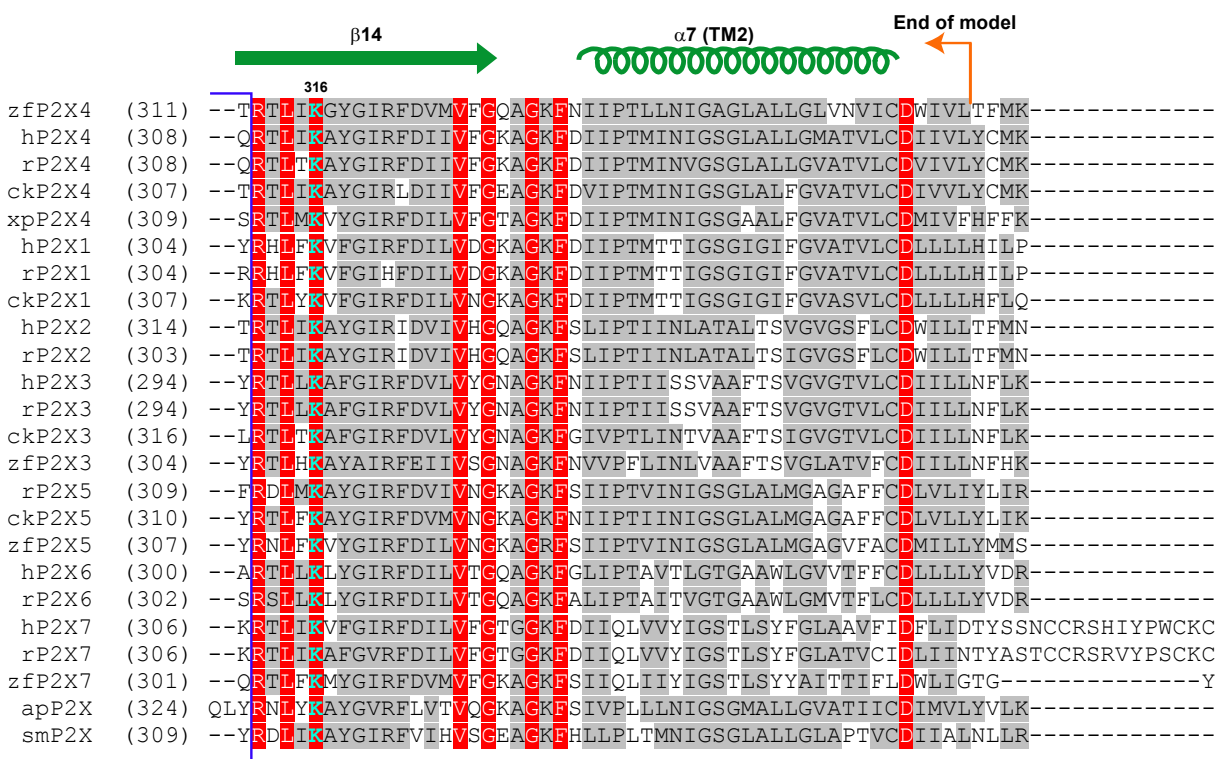
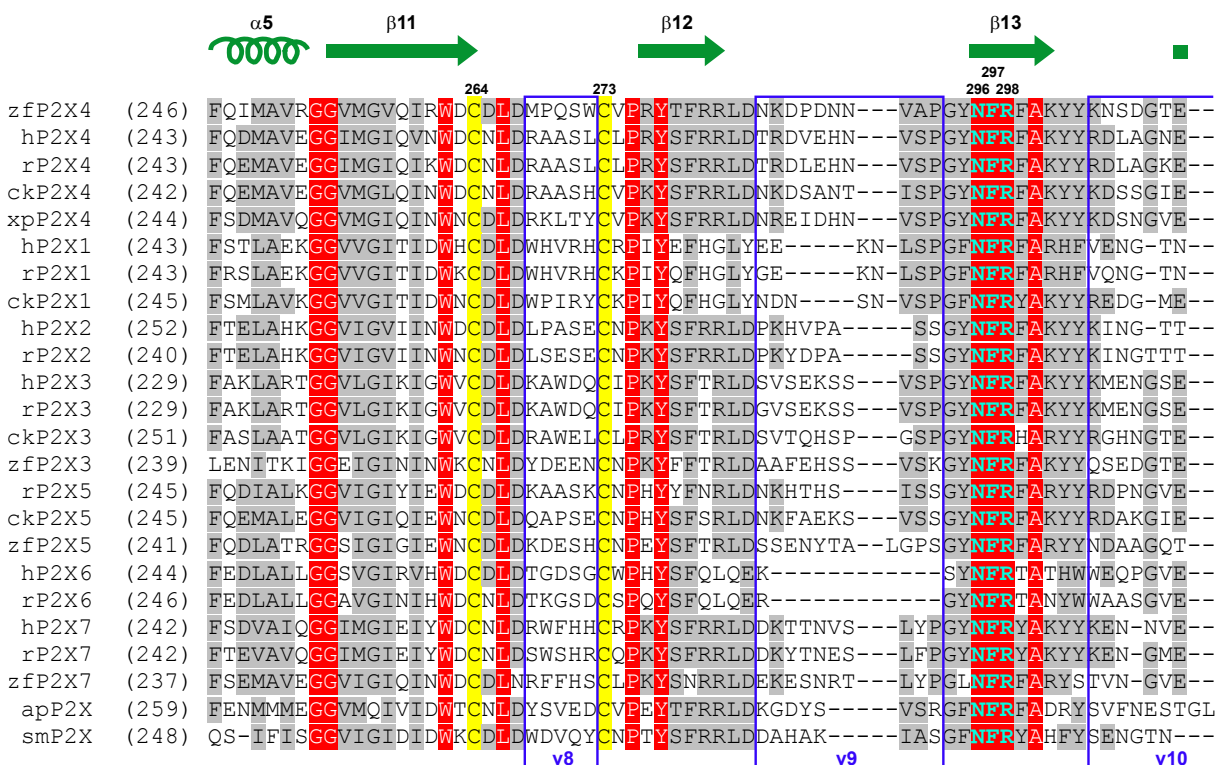
Supplementary Fig. 1. P2X receptors are glycosylated and tend to aggregate. **a,b,** Western blot analysis showing that rat P2X4 (rP2X4) is a trimer before solubilization (**a**) and after solubilization only in digitonin but not in dodecyl-maltoside (DDM), β -octyl-glucoside, or CHAPS (**b**). The membrane fraction from T-REx293 cells expressing rP2X4 was isolated by homogenization followed by centrifugation at 66,000 \times g for 40 min. The resulting pellet was cross-linked with glutaraldehyde (GA) at room temperature for 30 min, either directly or after solubilization in different detergents. Cross-linked products were analyzed by colorimetric Western blot using anti-His primary antibody. Lanes 1-6 indicate cross-linking with increasing concentrations of GA (0, 50 μ M, 250 μ M, 2.5 mM, and 25 mM, respectively). After solubilization with DDM (lanes 7-10), n-octyl- β -D-glucoside (lanes 11-14), CHAPS (lanes 15-18), or digitonin (lanes 19-22), rP2X4 was cross-linked with increasing concentrations of GA (0, 50 μ M, 500 μ M, and 5 mM, respectively). **c-f,** Negatively stained electron micrograph. rP2X4 was purified either in 1 mM DDM (**c, d**) or 0.5 % digitonin (**e, f**), applied to carbon-coated copper grids, stained with 2 % uranyl acetate, cooled with liquid nitrogen, and observed using a Tecnai G2 F20 cryo-electron microscope at 50,000 \times magnification. **d** and **f** are magnified images of the yellow squares in **c** and **e**, respectively. **g,** Affinity purified Δ zfP2X4 was treated with (+) and without (-) endoglycosidase H (Endo H), cleaved with thrombin, further purified by size exclusion chromatography, resolved by SDS-PAGE and stained with Coomassie Brilliant Blue.



Supplementary Fig. 2. ATP dose-dependent activation and expression levels of zfP2X4 constructs. **a**, ATP dose-dependent activation of zfP2X4.1-EGFP (light grey, EC_{50} = 1730 μM , Hill slope (n) = 0.9), $\Delta\text{zfP2X4-A-EGFP}$ (black, EC_{50} = 27.4 μM , n = 1.6) and $\Delta\text{zfP2X4-B-EGFP}$ (blue, EC_{50} = 3.4 μM , n = 1.3) determined from whole cell, patch-clamp recordings. Peak ATP evoked current amplitudes were measured for a range of ATP concentrations and fit using the Hill equation. Data are displayed normalized to the maximum current (I_{max}) estimated by the best fit of the Hill equation. Error bars indicate s.e.m. for 3-6 cells. **b-d**, Equal numbers of tsA201 cells (250,000) were transfected with 1 μg of the zfP2X4.1-EGFP construct (**b**), the $\Delta\text{zfP2X4-A}$ construct (**c**), or the $\Delta\text{zfP2X4-B}$ construct (**d**). Bright field (left panels) and epifluorescent (right panels) images were photographed 36 hours post-transfection.

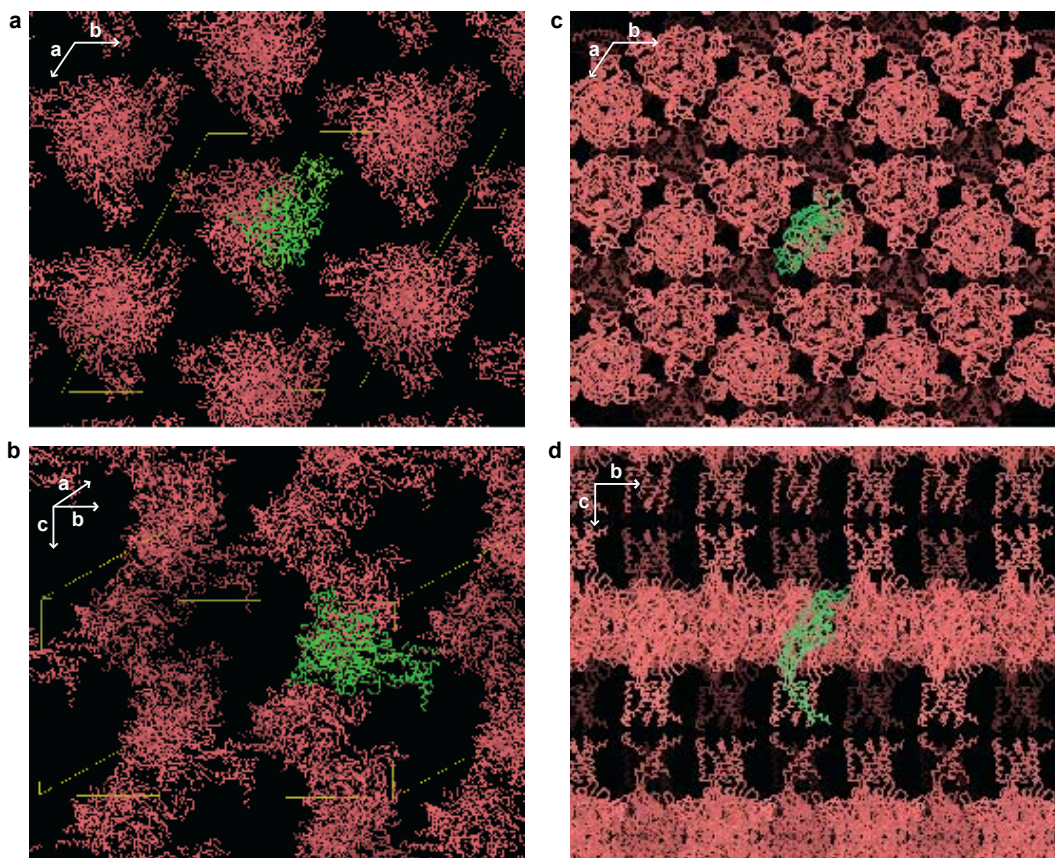




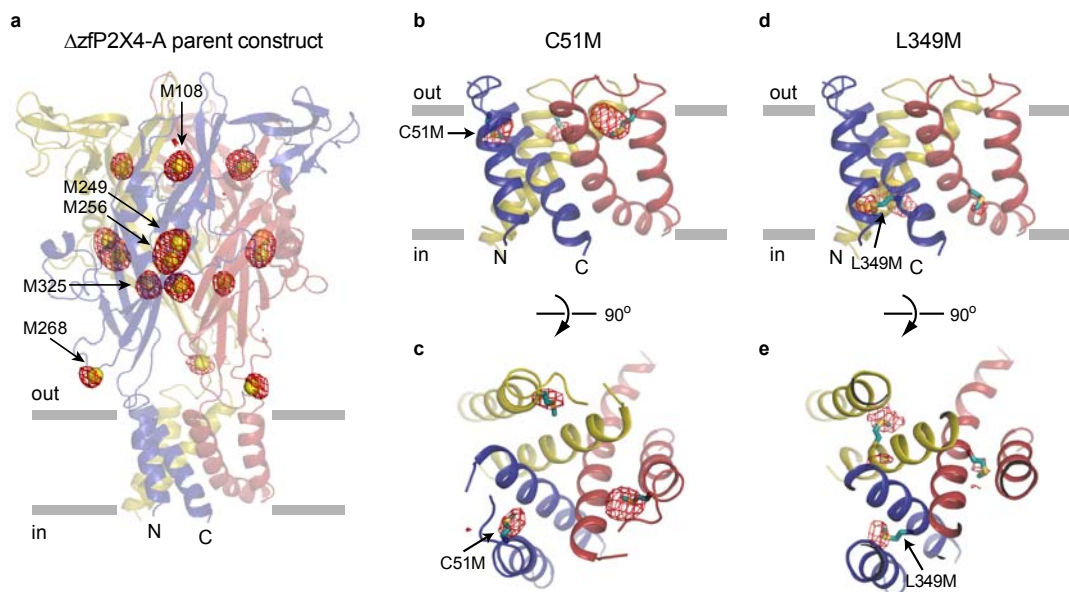




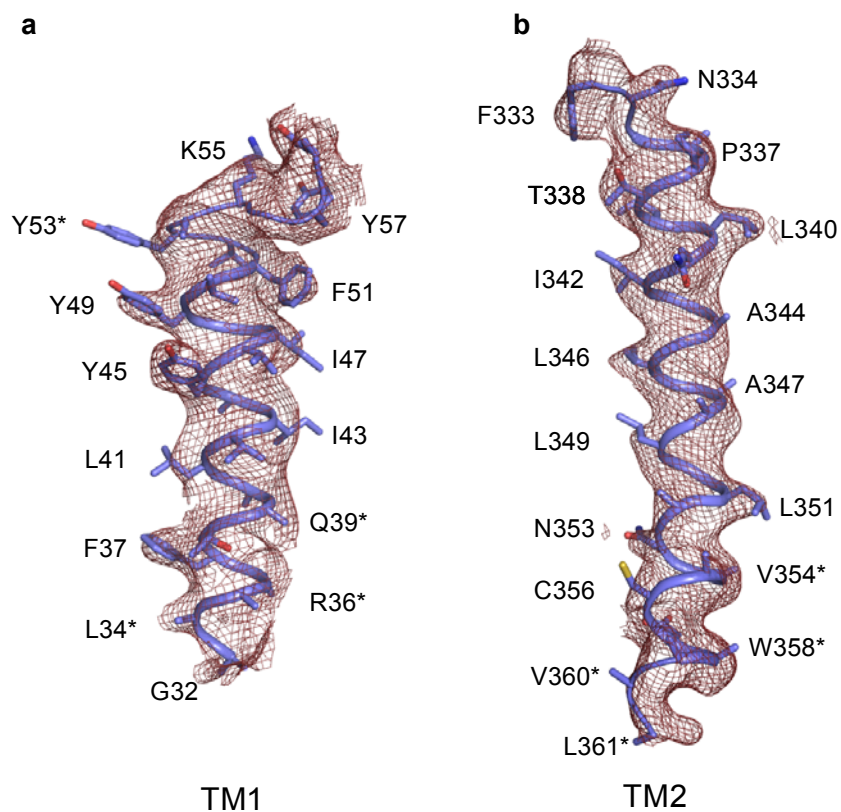
Supplementary Fig. 3. Sequence alignment. Sequence alignment of P2X receptors from zebrafish (zfP2X4.1, GI: 12656589; zfP2X4.2, 33520721; zfP2X3, 7542523; zfP2X5, 21667663; and zfP2X7, 33520711), human (hP2X1, 4505545; hP2X2, 25092719; hP2X3, 28416925; hP2X4, 116242696; hP2X6, 6469324; and hP2X7, 29294631), rat (rP2X1, 1352689; rP2X2, 18093098; rP2X3, 1030065; rP2X4, 1161345; rP2X5, 1279659; rP2X6, 1279661; and rP2X7, 1322005), chicken (ckP2X1, 45383135; ckP2X3, 118091425; ckP2X4, 82223288; and ckP2X5, 82217039), African clawed frog (xpP2X4, 12007266), sea slug (apP2X, 39578339), and blood fluke (smP2X, 51988420). Starting and ending residues of Δ zfP2X4 construct and the current model are indicated with orange arrows. Secondary structure elements are depicted in cartoon representation and are labeled as in Figure 3a. The sequence alignment was made using Vector NTI. Conserved cysteine residues are highlighted in yellow, other conserved residues are in red, and less conserved residues are in grey. The four glycosylated asparagines are labeled as in Figure 3a and are highlighted in green.



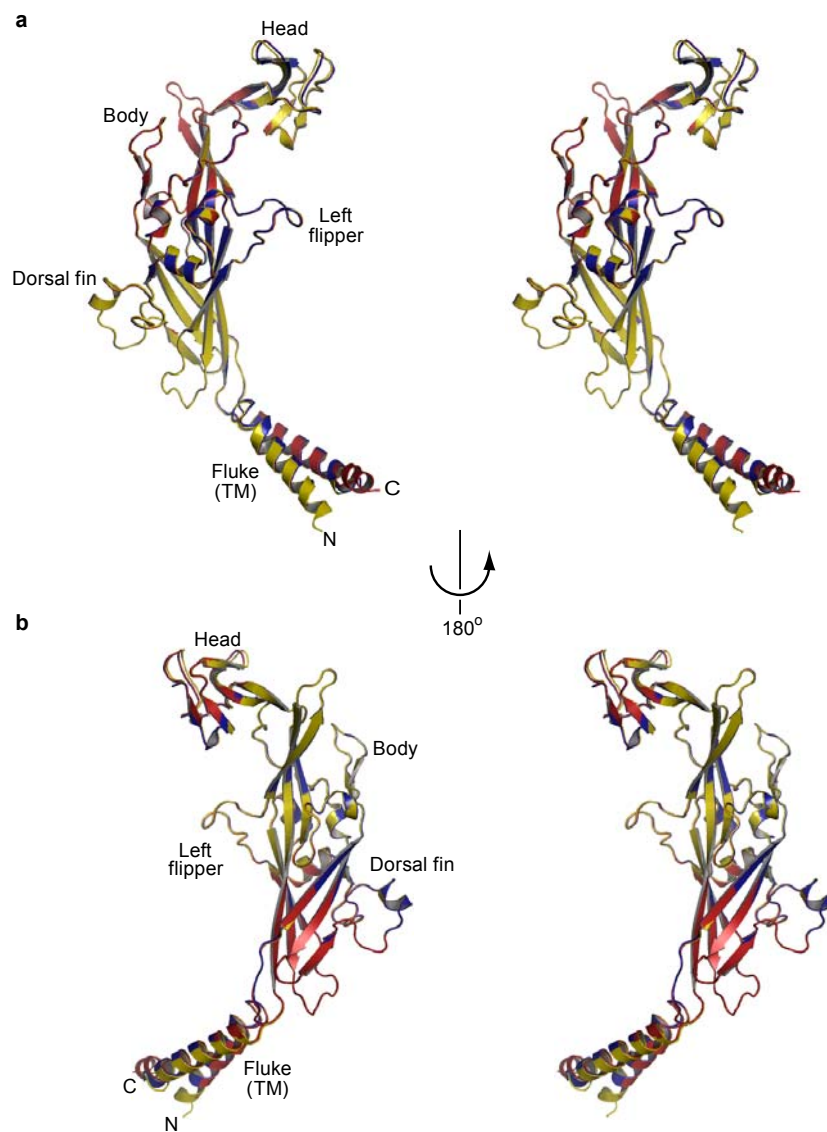
Supplementary Fig. 4. Crystal packing of Δ zfP2X4 constructs. **a, b**, Packing of receptors in the R3 space group. Δ zfP2X4-A crystals viewed perpendicular to the a-b plane (**a**) and perpendicular to the b-c plane (**b**). The unit cell (hexagonal setting) is shown in yellow. **c, d**, Packing of receptors in the R32 space group. Δ zfP2X4-B crystals viewed perpendicular to the a-b plane (**c**) and perpendicular to the b-c plane (**d**). Symmetrically-related molecules are represented as Ca traces in red, with one crystallographic unique molecule or subunit shown in green.



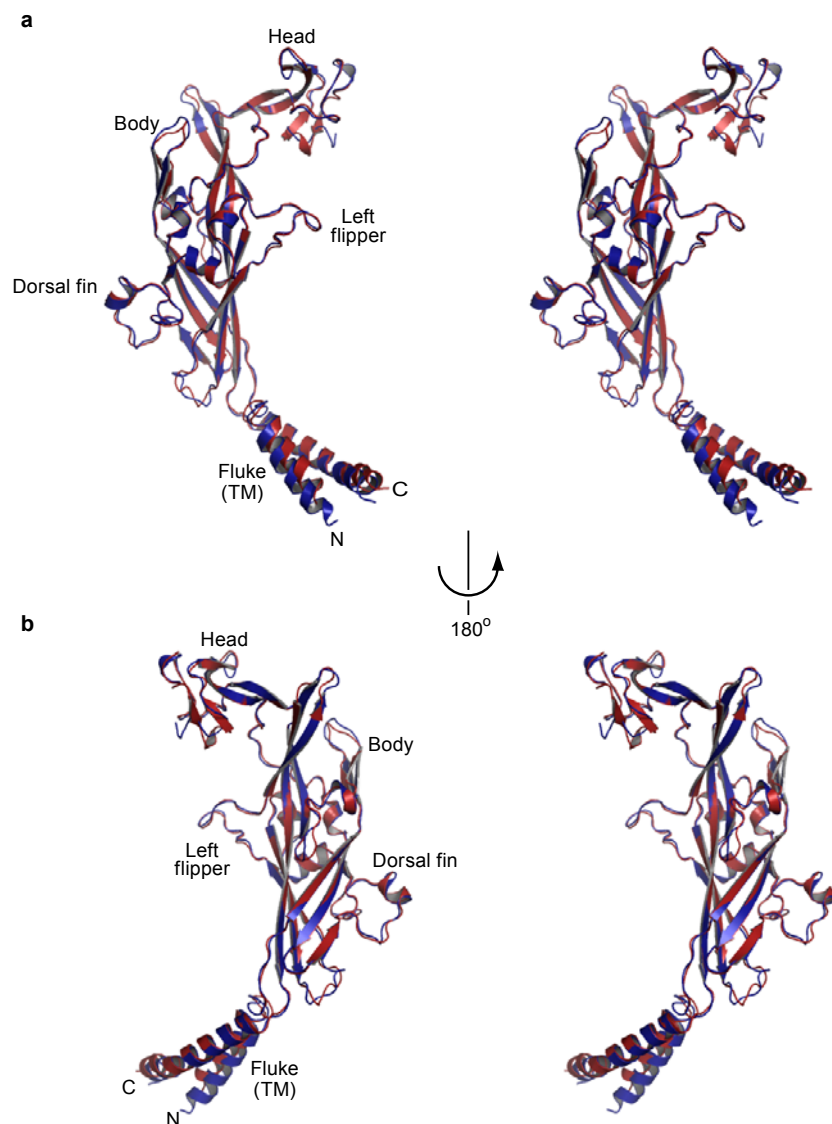
Supplementary Fig. 5. Anomalous difference Fourier maps from selenomethionine derivatives of Δ zfP2X4-A. **a**, An anomalous difference map from a selenomethionine derivative of the parent Δ zfP2X4-A contoured at 3.6σ (red) confirms the location of methionine residues. The methionine sulfur atoms are yellow spheres. **b-e**, Anomalous difference maps from selenomethionine derivatives of the C51M (**b, c**) and L349M constructs (**d, e**) contoured at 3.0σ (red) confirm the assignment of residues on the transmembrane helices. Predicted locations of the mutated methionine residues are shown in stick representation.



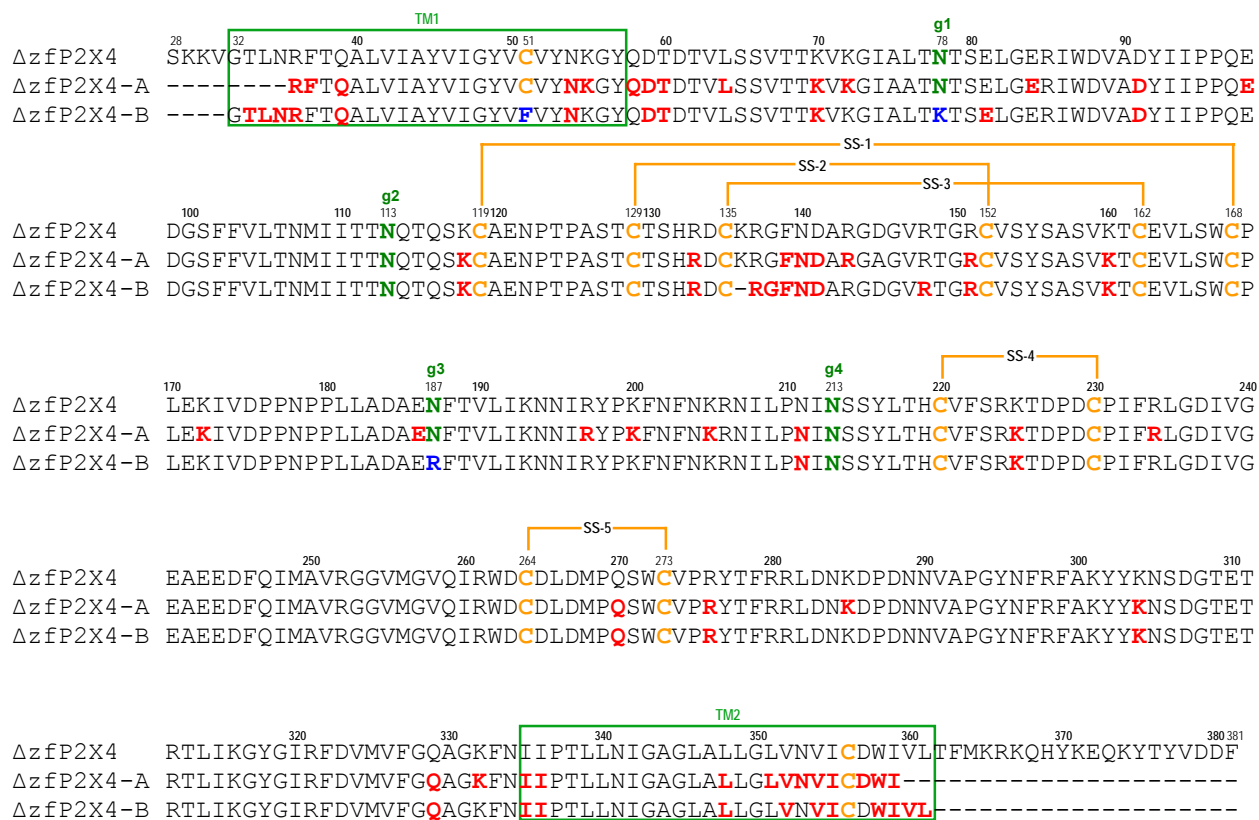
Supplementary Fig. 6. Electron densities in the transmembrane regions from the Δ zfP2X4-B crystal structure. Shown are 2Fo-Fc maps contoured at 0.8 for TM1 (a) and TM2 (b). The residues with weak side chain densities (asterisked), except for Y53, are shown as alanine.



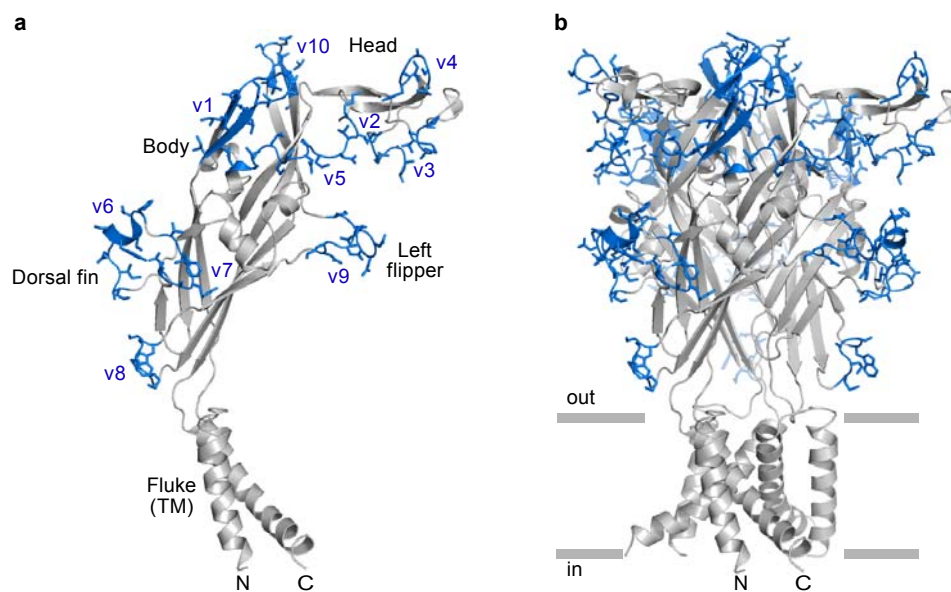
Supplementary Fig. 7. Stereoview of a superposition of the three crystallographically independent subunits from the Δ zfP2X4-A (R3) crystal form. **a, Subunit B (red) and C (yellow) are superimposed onto subunit A (blue) using C α positions in the extracellular region. **b**, Superposition as viewed along the non-crystallographic three-fold axis rotated 180° from **a**.**



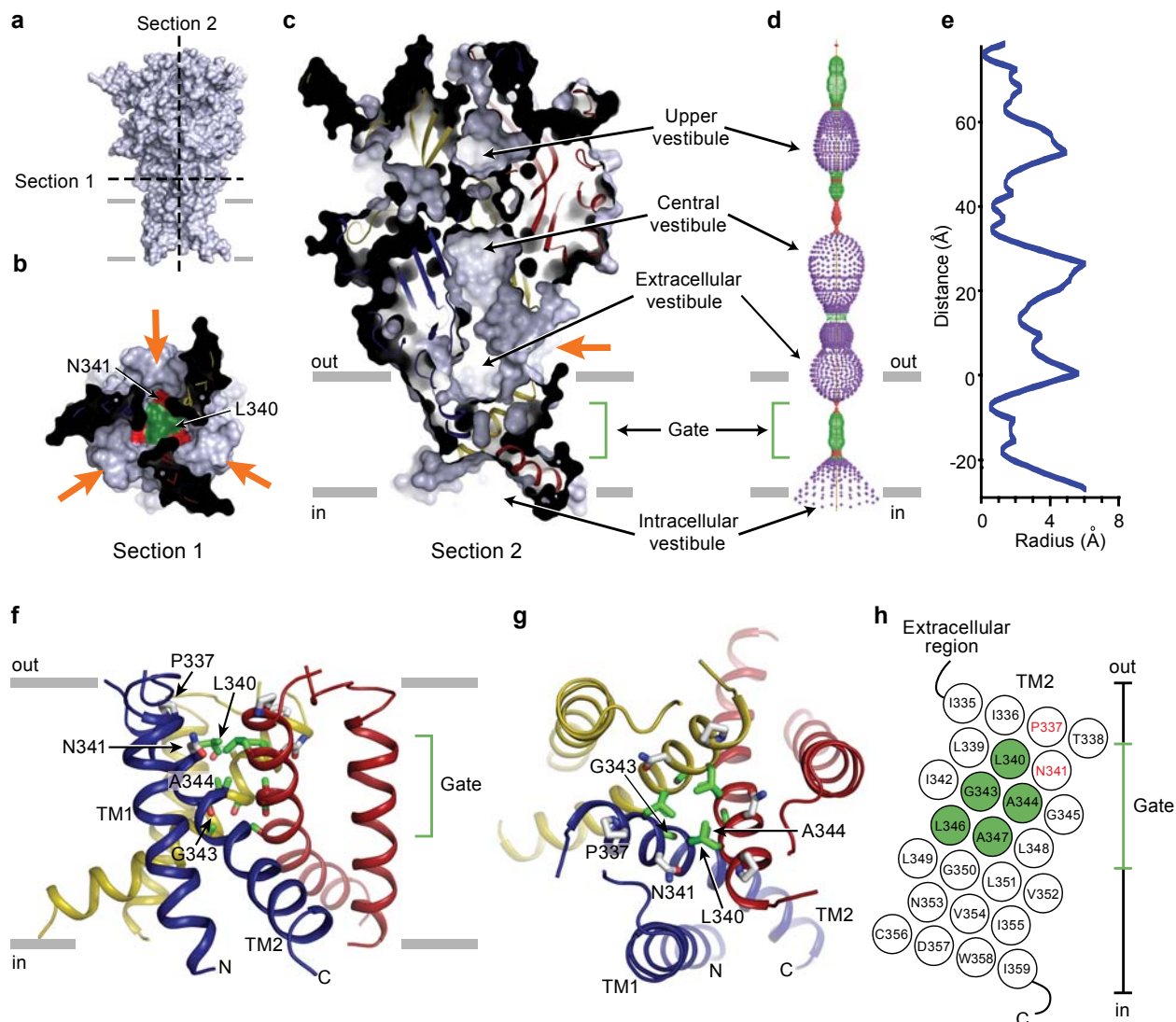
Supplementary Fig. 8. Stereoview of the subunit superposition between the Δ zfP2X4-A and Δ zfP2X4-B crystal structures. a, Δ zfP2X4-A Subunit A (red) is superimposed onto a Δ zfP2X4-B protomer (blue) using C α positions in the extracellular region. b, Superposition as viewed along the non-crystallographic three-fold axis rotated 180° from a.



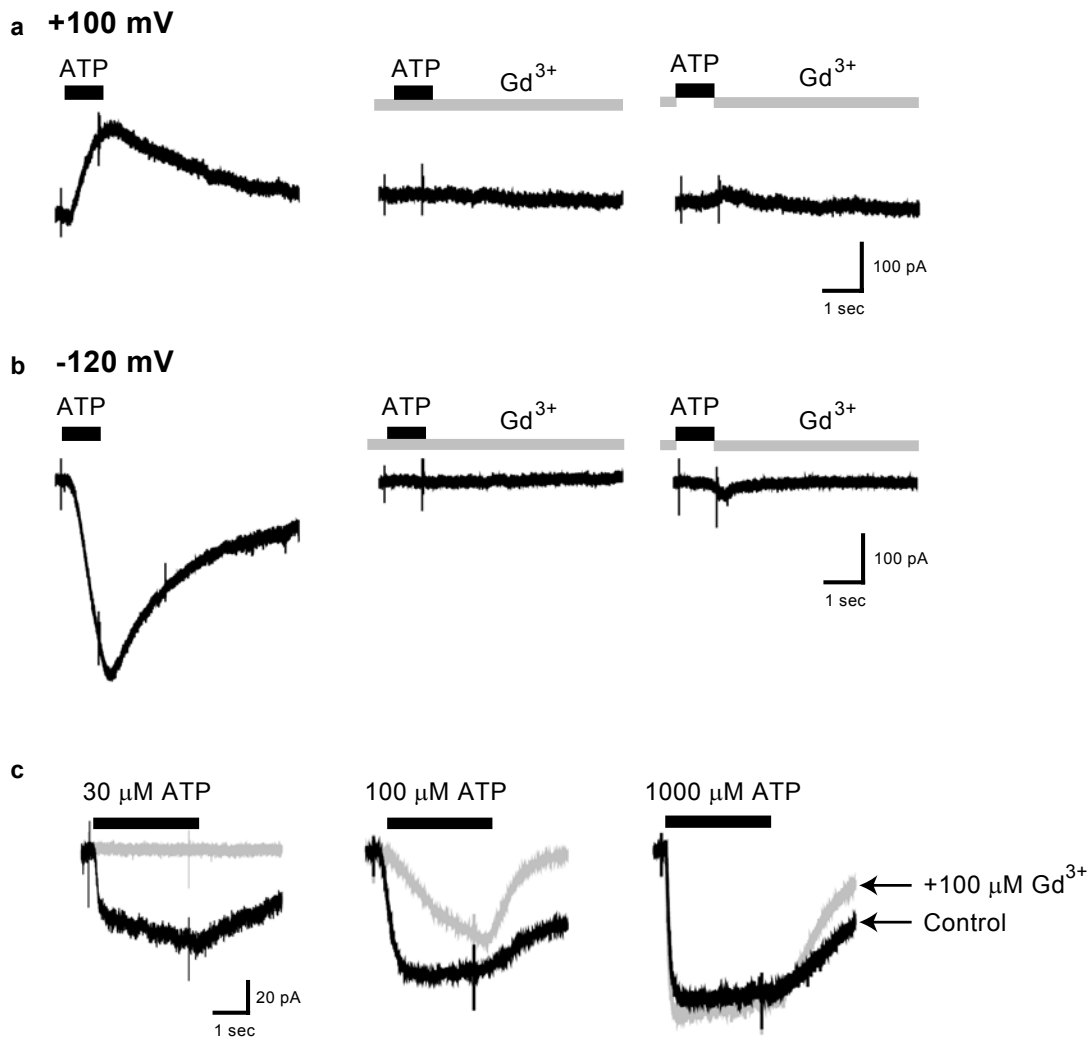
Supplementary Fig. 9. Sequence and features of the constructs used in the current structural study. The $\Delta z f P 2 X 4$ construct was used to form the $\Delta z f P 2 X 4 - A$ (R3 space group) crystals. The sequence labeled as $\Delta z f P 2 X 4 - A$ defines the residues from one of the three crystallographically independent subunits (A chain) in the $\Delta z f P 2 X 4 - A$ crystal structure. The residues without clear main chain electron densities are not included in the crystal structure and are shown here as dashed lines; the residues with weak side chain densities are built as alanines in the structure and are shown in red letters. To produce the $\Delta z f P 2 X 4 - B$ construct we made the following mutations: C51F, N78K, and N187R; the changes in amino acid residues are shown in blue. Cysteine residues are depicted in orange and disulfide bonded pairs are indicated. The green boxes labeled TM1 and TM2 are the α -helical transmembrane regions based on the crystal structures.



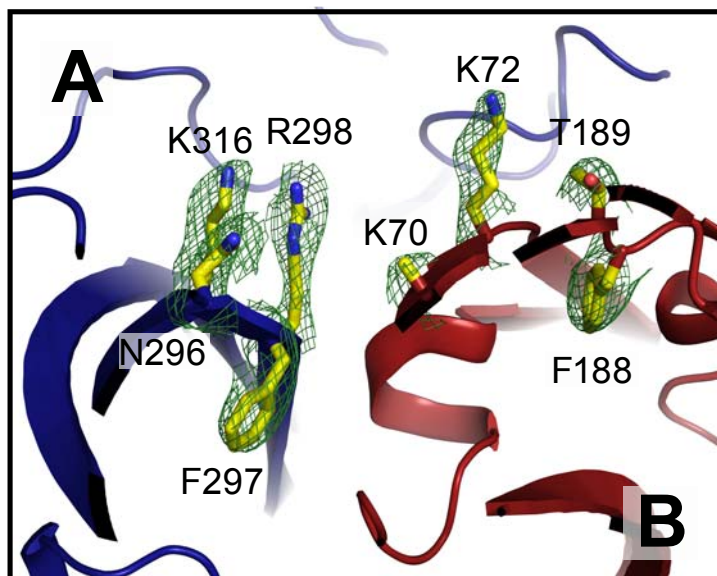
Supplementary Fig. 10. The locations of variable residues. Stretches of five or more non-conserved residues are highlighted in blue. **a**, A single protomer. **b**, The assembled trimer.



Supplementary Fig. 11. Extracellular vestibules and the ion channel domain. **a**, Sections of the receptor parallel (section 1) and perpendicular (section 2) to the membrane. **b**, Possible ion pathways are highlighted with orange arrows. Solvent facing residues in TM2 (L340, green and N341, red) are coloured differently. **c**, Section 2 reveals a closed conformation of the pore and shows that the gate is located about halfway across the membrane bilayer. Three vestibules (upper, central and extracellular vestibules) are located on the molecular 3-fold axis, with the extracellular vestibule connected to the bulk solution through a fenestration (orange arrow). **d**, Pore lining surface calculated by the Hole⁴⁹ program. Each colour represents a different radius range measured from the receptor centre (red: <1.15 Å, green: 1.15-2.3 Å, and purple: >2.3 Å). **e**, Pore radius plotted against the distance from the extracellular membrane boundary. **f**, Cartoon representations of the transmembrane domain viewed parallel to the membrane plane. P337 and N341 are shown in grey and potential gate residues (L340, G343, A344, and A347) are shown in green. **g**, Transmembrane domain viewed perpendicular to the membrane plane. **h**, Helical net diagram of TM2. Residues that occlude the transmembrane pore are depicted in green. Residues analogous to gating residues in cASICmfc are in red font.



Supplementary Fig. 12. Gadolinium inhibits ATP-evoked currents in a concentration dependent, voltage independent manner and accelerates the rate of deactivation. a, b, ATP (30 μM, 1 sec) was applied at positive (+100 mV, **a**) and negative (-120 mV, **b**) membrane potentials. ATP-evoked currents were completely blocked when 100 μM GdCl₃ was present in both control and ATP-containing test solutions (middle traces), indicating that inhibition of currents was voltage independent. Furthermore, the presence of 100 μM GdCl₃ only in the control solution and not in the ATP-containing test solution (right traces) was sufficient to largely abolish the ATP evoked currents, suggesting that sequestration of ATP by gadolinium was not responsible for the inhibition. Scale: 100 pA, 1 sec. **c,** ATP (3 sec) was applied at varying concentrations in the absence (black) or presence (grey) of 100 μM GdCl₃. Gadolinium was present in both the bath and ATP-containing solutions when applied. Gadolinium completely abolished currents evoked by 30 μM ATP and partially inhibited currents evoked by 100 μM ATP while currents evoked by 1 mM ATP were seemingly unaffected. Also note the increased rate of deactivation in the presence of gadolinium. Scale: 20 pA, 1 sec.



Supplementary Fig. 13. Side chain density in the ATP-binding pocket viewed $\sim 90^\circ$ from Figure 6b. Conserved residues previously proposed to be involved in ATP binding are labeled, and side chains are presented in stick representation in yellow. 2Fo-Fc electron density maps around the side chains are depicted in green. K70 is shown as an alanine due to an ambiguous side chain density.